

Magnon-Mediated Hall Effect in Kagomé Antiferromagnets

S. A. Owerre^{1,2}

¹*Perimeter Institute for Theoretical Physics, 31 Caroline St. N., Waterloo, Ontario N2L 2Y5, Canada.*

²*African Institute for Mathematical Sciences, 6 Melrose Road, Muizenberg, Cape Town 7945, South Africa.*

(Dated: July 28, 2022)

Many frustrated magnets at high magnetic field show evidence of magnetic order as confirmed in various experiments. In this Letter, we present a theoretical investigation of thermal Hall effect of spin excitations in Kagomé antiferromagnets with Dzyaloshinsky-Moriya interaction (DMI) subject to a magnetic field. We show that this system exhibits a finite thermal Hall conductivity (κ_{xy}). Interestingly, for the coplanar 120° Néel order subject to an external magnetic field, κ_{xy} is finite even at zero DMI in stark contrast to ferromagnets. Remarkably, the profile of κ_{xy} captures the trend seen in recent experiment in frustrated Kagomé volborthite $\text{Cu}_3\text{V}_2\text{O}_7(\text{OH})_2 \cdot 2\text{H}_2\text{O}$ at strong magnetic field. We propose other experimentally accessible Kagomé antiferromagnetic crystals as potential candidates for observing this effect.

PACS numbers: 66.70.-f, 75.10.Jm

In the classical Hall effect [1] a magnetic field \mathbf{B} is applied perpendicular to the current \mathbf{J}_e direction in a metal, as a result the current experiences a Lorentz force $\mathbf{F} = \mathbf{q} \cdot (\mathbf{v} \times \mathbf{B})$. The propagation of current is deflected in circular cyclotron orbits by the Lorentz force and charges accumulate on the edge of the material which causes a voltage difference called the Hall voltage. In the quantum case the magnetic orbits are quantized as Landau levels and give rise to a quantized Hall conductivity termed the integer quantum Hall effect [2–4]. Besides, the topology of the electron bands can lead to interesting phenomenon without the influence of the magnetic field. This induces nonzero Berry curvatures and Chern numbers leading to a quantized Hall conductivity termed quantum anomalous Hall effect [5].

The magnetic excitations of ordered quantum magnetic systems are bosonic quasiparticles known as magnons. In these systems the DMI [6] is possible if the magnetic crystal lacks inversion symmetry. The Kagomé lattice is built with this property because the midpoints between the bonds connecting the lattice sites are not center of inversion. The DMI leads to nontrivial topological magnon bands and Berry curvatures in ferromagnets [7–15] similar to electronic systems. As magnons are charged-neutral quasiparticles they do not experience the magnetic field in the Lorentz force as in charged particles. Instead, a temperature gradient $-\nabla T$ transports a heat current \mathbf{J}_Q and the DMI-induced Berry curvature acts as an effective magnetic field that deflects the propagation of magnons in the system. The response of the system due to $-\nabla T$ gives rise to a thermal analog of the Hall effect characterized by a temperature-dependent thermal Hall conductivity tensor κ_{ij} [7, 8]. Thermal Hall effect of magnons and DMI-induced band topology have been studied extensively in single-layer Kagomé ferromagnets [7–13, 16, 17]. They were recently observed in effectively two-dimensional (2D) Kagomé magnet Cu(1-3, bdc) [18, 19] and previously reported

in 3D pyrochlore ferromagnets $\text{Lu}_2\text{V}_2\text{O}_7$, $\text{Ho}_2\text{V}_2\text{O}_7$, and $\text{In}_2\text{Mn}_2\text{O}_7$ [20, 21].

In this Letter, we study a different system with antiferromagnetic coupling. The motivation for undertaking this investigation is two-fold. First, thermal Hall response of stacked Kagomé magnetic systems has received no attention, although several stacked Kagomé materials occur in nature. In fact, the Kagomé magnet Cu(1-3, bdc)[18, 19] is an antiferromagnetically-coupled stacked Kagomé ferromagnets. Owing to weak interlayer antiferromagnetic exchange between planes $J_t \sim 1p$ meV, this system is effectively a single-layer Kagomé ferromagnet [18, 19]. Interestingly, there are other stacked Kagomé magnetic systems [23, 24] with sufficiently large interlayer coupling such as $\text{Ca}_{10}\text{Cr}_7\text{O}_{28}$ with a ferromagnetic interlayer exchange $J_t \sim -0.08$ meV [23]. Evidently, magnetic materials of this nature cannot be approximated as a single-layer system due to large interlayer coupling, and the associated thermal Hall response will differ significantly from those of single-layer systems.

Second, we have recently learnt about the experimental observation of thermal Hall response in frustrated 2D distorted Kagomé volborthite $\text{Cu}_3\text{V}_2\text{O}_7(\text{OH})_2 \cdot 2\text{H}_2\text{O}$ [22]. A transverse thermal Hall conductivity was observed in a strong magnetic field ($B_z \sim 15T$) and its signal is attributed to spin excitations in the spin liquid (SL) phase. However, a strong field of this magnitude is sufficient to cause magnetic order in this crystal [25, 26]. Also in a recent study [23], it has been shown that strong magnetic field is sufficient to circumvent frustrated interactions and leads to magnetic order in frustrated Kagomé compound $\text{Ca}_{10}\text{Cr}_7\text{O}_{28}$. As we show in this Letter, the coplanar 120° Néel structure on the Kagomé lattice with out-of-plane DMI [27–32] shows vanishing/negligible κ_{xy} at zero field as opposed to ferromagnets with DMI [7–9, 12, 13, 16–19]. We show that the magnetic field induces a chiral interaction that gives rise to nonzero κ_{xy} even in the absence of DMI. For these reasons, there is a

possibility of magnon-mediated thermal Hall response in spin-1/2 Kagomé antiferromagnets in which various compounds with DMI have been synthesized [27–32]. This Letter provides a theoretical background that will simulate present and upcoming experimental materials with finite thermal Hall response.

We consider stacked Kagomé magnetic systems with symmetry breaking DMI and non-negligible interlayer coupling. Without loss of generality, we consider a single stacked Kagomé planes (bilayer Kagomé planes) and we assume that the top layer is placed right above the bottom layer forming AA-stacked pattern. The Hamiltonian is given by

$$H = \sum_{\langle i,j \rangle} [J\mathbf{S}_i^\tau \cdot \mathbf{S}_j^\tau + \mathbf{D}_{ij} \cdot \mathbf{S}_i^\tau \times \mathbf{S}_j^\tau] - g\mu_B \mathbf{B} \cdot \sum_i \mathbf{S}_i^\tau + J_t \sum_i \mathbf{S}_i^T \cdot \mathbf{S}_i^B, \quad (1)$$

where \mathbf{S}_i is the spin moment at site i , τ labels that top (T) and bottom (B) layers respectively, g is the g -factor and μ_B is the Bohr magneton, \mathbf{B} is an external magnetic field. The inversion symmetry breaking in this system gives rise to a DM vector \mathbf{D}_{ij} .

We consider three different cases: (i) layer ferromagnet: $J, J_t < 0$, (ii) layer antiferromagnet: $J < 0, J_t > 0$, and (iii) pure antiferromagnetic insulator: $J, J_t > 0$. Case (i) is applicable to the Kagomé compound $\text{Ca}_{10}\text{Cr}_7\text{O}_{28}$, since a high magnetic field is sufficient to circumvent the frustrated interactions and forces the spins to align in the direction of the external field [23]. It is also applicable to a variant of $\text{Cu}(1-3, \text{bdc})$ with strong interlayer coupling, since a small out-of-plane field is sufficient to align the spins along the field direction [18, 19]. Case (ii) is applicable to systems in which the spins on the top and bottom layers are oriented in different directions. For these cases the interlayer and intra-layer couplings do not introduce spin frustration. However, case (iii) exhibits spin frustration at zero field due to intra-layer antiferromagnetic couplings. Nevertheless, it has been pointed out that an out-of-plane DMI induces magnetic order (coplanar 120° structure) in the single-layer Kagomé antiferromagnets [27–33]. We believe that the 120° coplanar structure persists for the bilayer system. For this magnetic order the interlayer coupling is ferromagnetic, unless the DMI has a different sign on both layers in which the interlayer coupling becomes antiferromagnetic.

At zero field the spins are along the Kagomé planes. For case (ii), the spins on the top layer are along the positive direction and those on the bottom layer are along the negative direction. The interlayer coupling is antiferromagnetic. As the out-of-plane magnetic field is turned on, the spins cant towards the direction of the field as shown in Figs. 1 (a) and (b). Hence, we shall start with

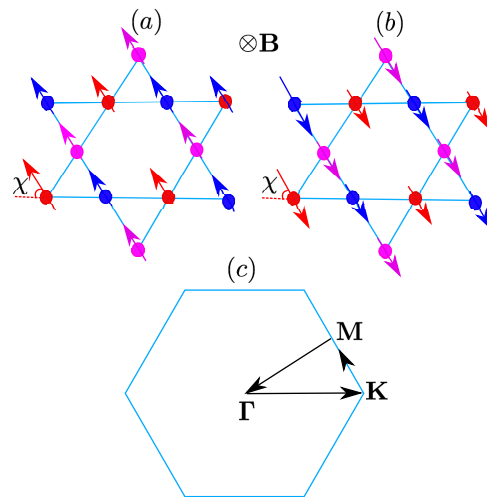


FIG. 1: Color online. Schematics of (a) canted spins on the top layer (b) canted spins on the bottom layer. The magnetic field is applied perpendicular to the plane. (c) The Brillouin zone indicating the high symmetry paths.

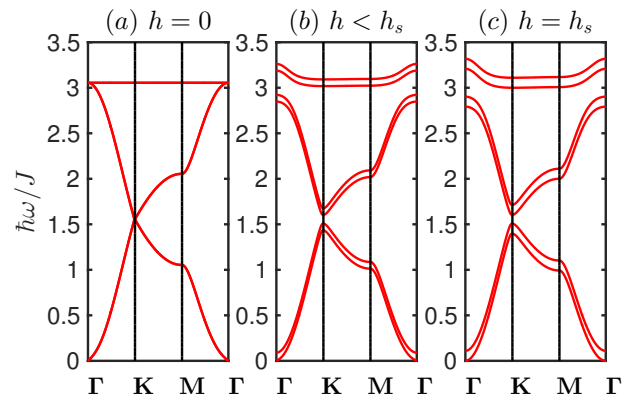


FIG. 2: Color online. Magnon bands of spin-1/2 stacked Kagomé antiferromagnet with $\mathbf{D} \parallel \mathbf{B}$ at several field values. The parameters are $D/J = 0.12$, $J_t/J = 0.11$.

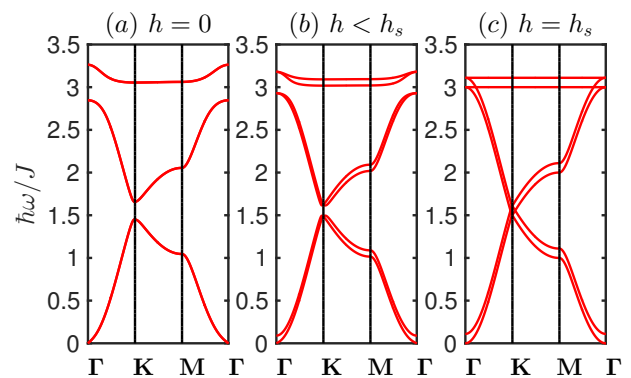


FIG. 3: Color online. Magnon bands of spin-1/2 stacked Kagomé antiferromagnet with $\mathbf{D} \perp \mathbf{B}$ at several field values. The parameters are $D/J = 0.12$, $J_t/J = 0.11$.

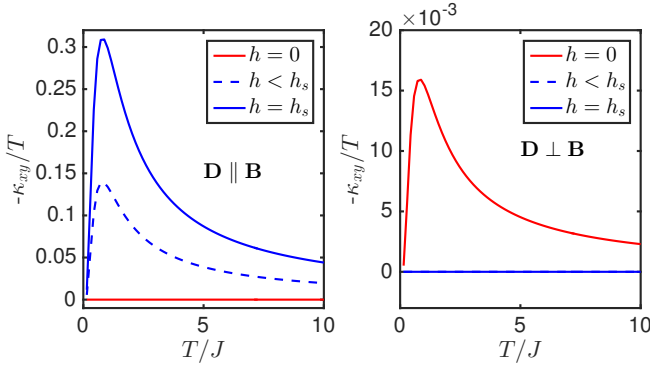


FIG. 4: Color online. Low-temperature dependence of κ_{xy} in stacked spin-1/2 Kagomé antiferromagnet for several field values: (a) $\mathbf{D} \parallel \mathbf{B}$. (b) $\mathbf{D} \perp \mathbf{B}$. The parameters are $D/J = 0.12$, $J_t/J = 0.11$.

case (ii) as it recovers case (i) at the saturation field. To capture the correct magnetic excitations, we have to rotate the coordinate axes on each layer such that the z -axis coincides with the local direction of the classical polarization. The appropriate rotation on each layer is given by

$$\begin{aligned} S_{i\tau}^x &= \pm S_{i\tau}^{l_x} \sin \chi \pm S_{i\tau}^{l_z} \cos \chi, \\ S_{i\tau}^y &= \pm S_{i\tau}^{l_y}, \\ S_{i\tau}^z &= -S_{i\tau}^{l_x} \cos \chi + S_{i\tau}^{l_z} \sin \chi, \end{aligned} \quad (2)$$

where $+$ ($-$) applies to the layers T (B) respectively. This rotation does not affect the ferromagnetic J -term on each layer. An interesting property of this system is that both the out-of-plane DMI ($\mathbf{D} = D\mathbf{z}$) and the in-plane DMI ($\mathbf{D} = D\mathbf{x}$) contribute to linear order in spin wave theory [34] valid at low temperatures. For $\mathbf{D} \parallel \mathbf{B}$, the rotation in Eq. 2 rescales the DMI as $D_l \rightarrow D \sin \chi$. On the other hand, for $\mathbf{D} \perp \mathbf{B}$, we have $D_t \rightarrow D \cos \chi$, where the subscripts $l(t)$ denote longitudinal (transverse) components of the DMI along the field direction. However, the DMI does not contribute to the classical energy given by

$$E_{cl}/6N = -|J|S^2 - \frac{J_t S^2}{2} \cos 2\chi - hS \sin \chi, \quad (3)$$

where $h = g\mu_B B_z$ and $6N$ is the total number of sites. Minimizing the classical energy yields the canting angle $\sin \chi = h/(h_s = 2J_t S)$. The spin wave [34] Hamiltonian maps to a bosonic tight binding model. For $\mathbf{D} = D\mathbf{z}$ we have

$$\begin{aligned} H_{SW} &= v_0 \sum_i n_i - v_D \sum_{\langle ij \rangle} \left(e^{-i\phi_{ij}} b_i^\dagger b_j + h.c. \right) \\ &+ v_t \sum_{i \in T, j \in B} \left[(n_i + n_j) \cos 2\chi - (b_i^\dagger b_j + h.c.) \sin^2 \chi \right. \\ &\left. + (b_i^\dagger b_j^\dagger + h.c.) \cos^2 \chi \right], \end{aligned} \quad (4)$$

where $n_i = b_i^\dagger b_i$ is the occupation number, $v_0 = 4|J|S + h \sin \chi$, $v_D = S\sqrt{J^2 + D_l^2}$, $v_t = J_t S$. The fictitious magnetic flux in each triangle of the Kagomé lattice is given by $\phi_{ij} = \pm\phi = \arctan(D_l/|J|)$.

The interlayer exchange interaction couples sites on the bottom layer to their corresponding sites on the top layer. We identify sites on the bottom layer with the labels A, B, C and those on the top layer with A', B', C' . The momentum space Hamiltonian is given by

$$H_{SW} = \frac{1}{2} \sum_{\mathbf{k}} \Psi_{\mathbf{k}}^\dagger \cdot \mathcal{H}_{AFM}(\mathbf{k}) \cdot \Psi_{\mathbf{k}}, \quad (5)$$

where $\Psi_{\mathbf{k}}^\dagger = (\psi_{\mathbf{k}}^\dagger, \psi_{-\mathbf{k}})$, with $\psi_{\mathbf{k}}^\dagger = (b_{\mathbf{k}A}^\dagger, b_{\mathbf{k}B}^\dagger, b_{\mathbf{k}C}^\dagger, b_{\mathbf{k}A'}^\dagger, b_{\mathbf{k}B'}^\dagger, b_{\mathbf{k}C'}^\dagger)$.

$$\mathcal{H}_{AFM}(\mathbf{k}) = \begin{pmatrix} \mathbf{A}(\mathbf{k}, \phi) & \mathbf{B} \\ \mathbf{B} & \mathbf{A}(-\mathbf{k}, \phi) \end{pmatrix}, \quad (6)$$

where

$$\mathbf{A}(\mathbf{k}, \phi) = \begin{pmatrix} \mathbf{a}(\mathbf{k}, \phi) & \mathbf{b} \\ \mathbf{b} & \mathbf{a}(\mathbf{k}, \phi) \end{pmatrix}, \quad \mathbf{B} = \begin{pmatrix} 0 & \mathbf{c} \\ \mathbf{c} & 0 \end{pmatrix}, \quad (7)$$

and $\mathbf{a}(\mathbf{k}, \phi) = \tilde{v}_0 \mathbf{I}_{3 \times 3} - 2v_D \mathbf{\Lambda}(\mathbf{k}, \phi)$,

$$\mathbf{\Lambda}(\mathbf{k}, \phi) = \begin{pmatrix} 0 & \cos k_1 e^{-i\phi} & \cos k_3 e^{i\phi} \\ \cos k_1 e^{i\phi} & 0 & \cos k_2 e^{-i\phi} \\ \cos k_3 e^{-i\phi} & \cos k_2 e^{i\phi} & 0 \end{pmatrix}, \quad (8)$$

$$\mathbf{b} = -v_t \sin^2 \chi \mathbf{I}_{3 \times 3}, \quad \mathbf{c} = v_t \cos^2 \chi \mathbf{I}_{3 \times 3}, \quad (9)$$

where $\mathbf{I}_{3 \times 3}$ is a 3×3 identity matrix, $\tilde{v}_0 = 4|J|S + h \sin \chi + v_t \cos 2\chi = 4|J|S + v_t$, $k_i = \mathbf{k} \cdot \mathbf{p}_i$, $\mathbf{p}_1 = (1, 0)$, $\mathbf{p}_2 = (-1/2, \sqrt{3}/2)$, $\mathbf{p}_3 = (-1/2, -\sqrt{3}/2)$. For $\mathbf{D} = D\mathbf{x}$, the flux ϕ changes sign on the top layer and $D_l \rightarrow D_t$.

We have shown the magnon bands of the system in Figs. 2 and 3 along the Brillouin zone paths in Fig. 1 (c), with the parameter values of $\text{Ca}_{10}\text{Cr}_7\text{O}_{28}$, $J = 0.76$ meV, $J_t = 0.08$ meV [23] and the DM value of $\text{Cu}(1-3, \text{bdc})$ $D = 0.09$ meV [18, 19]. For $\mathbf{D} \parallel \mathbf{B}$ (Fig. 2) the DMI does not contribute at zero field $h = 0$ ($\chi = 0$) and the bands are doubly degenerate with one flat band and two dispersive bands gapless at the Dirac points $\mathbf{K} = (\pm 2\pi/3, 0)$. As the magnetic field increases from zero $h < h_s$, the spins on each layer cant along the field direction and the degeneracy of the bands is lifted. Thus, the DMI opens a gap at \mathbf{K} and the system is then topological with magnon edge states (not shown) propagating in the vicinity of the bulk gap. When the magnetic field approaches the saturation point $h = h_s$ each layer is fully polarized along the field direction, thus we recover layer ferromagnet (case i) with gapped magnon bands. For $\mathbf{D} \perp \mathbf{B}$ (Fig. 3) the situation is different. Although the bands are doubly degenerate at $h = 0$, the DMI does not disappear and the system is gapped. As usual, degeneracy is lifted with nonzero field and the DMI does

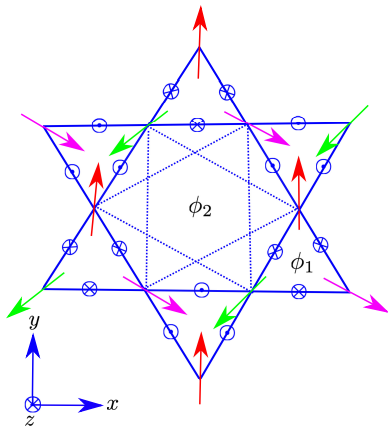


FIG. 5: Color online. The zero field coplanar 120° Néel order on the Kagomé lattice corresponding to the $\mathbf{q} = 0$ ground state of Kagomé antiferromagnet in the presence of an out-of-plane DMI. The dashed triangle connects the NNN sites. At nonzero field each spin cant by an angle χ with respect to the field. The coloured arrows denote different sublattices and $\phi_{1,2}$ are the field-induced fictitious fluxes on the NN and NNN triangular plaquettes.

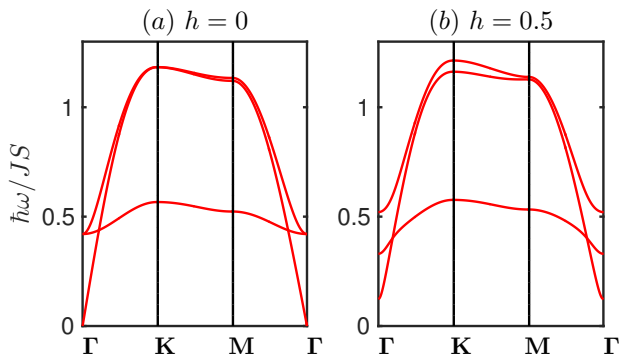


FIG. 6: Color online. Magnon bands of single-layer Kagomé antiferromagnet with $\mathbf{D} \parallel \mathbf{B}$ at two field values. The parameters are $D/J = 0.06$, $J_2/J = 0.03$ and $J = 3.34$ meV. This corresponds to the parameter values of $\text{KFe}_3(\text{OH})_6(\text{SO}_4)_2$ [28].

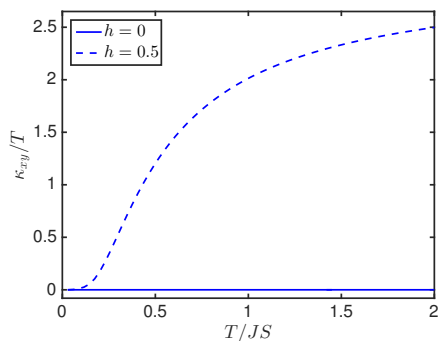


FIG. 7: Color online. Low-temperature dependence of κ_{xy} in Kagomé antiferromagnet for two field values and $D/J = 0.06$, $J_2/J = 0.03$, $J = 3.34$ meV.

not contribute at the saturation point $h = h_s$, with trivial band structures. As mentioned above, $\text{Ca}_{10}\text{Cr}_7\text{O}_{28}$ orders ferromagnetically at $h_s \sim 11T$ and $\text{Cu}(1-3, \text{bcd})$ orders ferromagnetically at $h_s \sim 0.05T$ assuming strong interlayer coupling.

The transverse thermal Hall conductivity κ_{xy} is plotted in Fig. 4 with the formula derived in Ref. [11]. For $\mathbf{D} \parallel \mathbf{B}$, the thermal Hall response κ_{xy}/T is negative and vanishes at zero field in accordance with the band structure in Fig. 2(a). In the interval $h \in (0, h_s]$, it shows a signal of nonzero values and develops a peak at $T \sim J$ before decreasing rapidly towards zero at high temperature. On the other hand, for $\mathbf{D} \perp \mathbf{B}$ the situation is different because the fictitious flux changes sign on the top layer. In this case κ_{xy} vanishes for $h < h_s$ and $h = h_s$, but shows evidence of nonzero value only at zero field. Quite surprisingly, the trends for $\mathbf{D} \parallel \mathbf{B}$ are similar to recent report of κ_{xy}/T on the frustrated Kagomé volborthite $\text{Cu}_3\text{V}_2\text{O}_7(\text{OH})_2 \cdot 2\text{H}_2\text{O}$ [22] at finite field. Although the DMI does not necessarily apply in the disordered SL regime, its effect is crucial in thermal Hall response once the system is ordered. It is quite possible that the strong magnetic field is sufficient to cause magnetic order in this crystal [23, 25, 26].

Finally, for case (iii) it suffices to consider single-layer antiferromagnet $J_t = 0$,

$$H = \sum_{i,j} J_{ij} \mathbf{S}_i \cdot \mathbf{S}_j + \sum_{\langle i,j \rangle} \mathbf{D}_{ij} \cdot \mathbf{S}_i \times \mathbf{S}_j - h \sum_i S_{iz}, \quad (10)$$

where $J_{ij} > 0$ are the isotropic antiferromagnetic couplings for nearest- (NN) and next-neighbours (NNN), $\mathbf{D}_{ij} = (0, 0, \mp D_z)$, where $-/+$ denotes the directions of the out-of-plane DMI in the up/down triangles as depicted in Fig. 5, and h is the magnetic field in units of $g\mu_B$. At zero magnetic field, the out-of-plane DMI induces a coplanar 120° Néel order on the Kagomé lattice [27–32]. However, the magnetic excitations of this Néel order do not exhibit nontrivial magnon bands even in the presence of DMI [28, 33]. It consists of one flat band (induced by the DMI) and two dispersive bands gapless at \mathbf{K} . This is reminiscent of Fig. 2(a). Hence, this zero field antiferromagnetic model is not expected to possess a finite thermal Hall response. As we have shown in the frustrated honeycomb lattice [35], an out-of-plane magnetic field can lead to finite thermal Hall response in frustrated antiferromagnets as corroborated in recent experiment [22]. The analysis for the Kagomé lattice is given in the Supplemental material.

For the Kagomé lattice, the magnetic field induces a chiral interaction of the form $H_\chi \sim \cos \chi (\mathbf{S}_i \times \mathbf{S}_j)_z$, where $\cos \chi = h/h_s$ with $h_s = [6(J + J_2) + \sqrt{3}D_z]S$. This chiral term generates fictitious fluxes on the NN and NNN triangular plaquettes as shown in Fig. 5. The magnon bands are shown in Fig. 6 with the parameter values of $\text{KFe}_3(\text{OH})_6(\text{SO}_4)_2$ [28] which has a negligible

interlayer coupling. We see that the bands develop a gap at \mathbf{K} and $\mathbf{\Gamma}$ with nonzero field. The low-temperature dependence of κ_{xy} is plotted in Fig. 7 with the parameter values of $\text{KFe}_3(\text{OH})_6(\text{SO}_4)_2$. We observe that κ_{xy} vanishes/negligible at zero field and a finite κ_{xy} is obtained for nonzero field. For zero DMI and $J_2 \neq 0$, we also observe a finite κ_{xy} (not shown). This can be easily understood since chirality is induced by the field and not the DMI. This is a crucial difference between the present antiferromagnetic model and previously studied ferromagnets [7–9, 12, 13, 18, 19] on the Kagomé lattice. This raises the possibility of finite thermal Hall response in various antiferromagnetic systems with/without DMI [27–32].

In summary, we have shown evidence of finite thermal Hall response in antiferromagnetically-coupled stacked Kagomé planes and Kagomé antiferromagnets. We showed that both the DMI and the magnetic field can lead to magnetic order with nontrivial excitations and nonzero thermal Hall conductivity is manifested. Interestingly, the results of our bilayer model show a similar trend recently seen in experiment on the Kagomé volborthite $\text{Cu}_3\text{V}_2\text{O}_7(\text{OH})_2 \cdot 2\text{H}_2\text{O}$ [22]. For the coplanar Néel order on the Kagomé lattice, we found that thermal Hall effect is present only at finite magnetic field and κ_{xy} shows a signal of nonzero value even with zero DMI. Our results also apply to bilayer pyrochlore ferromagnets and antiferromagnets which usually contain stacked Kagomé planes along the $\langle 111 \rangle$ direction. These results will simulate upcoming experimental Kagomé materials with finite thermal Hall response.

Research at Perimeter Institute is supported by the Government of Canada through Industry Canada and by the Province of Ontario through the Ministry of Research and Innovation.

-
- [1] E. H. Hall, American Journal of Mathematics **2**, No. 3 (1879), pp. 287-292.
- [2] K. v. Klitzing, G. Dorda, and M. Pepper, Phys. Rev. Lett. **45**, 494 (1980)
- [3] R. B. Laughlin, Phys. Rev. B **23**, 5632(R) (1981).
- [4] D. J. Thouless, M. Kohmoto, M. P. Nightingale, and M. den Nijs, Phys. Rev. Lett. **49**, 405 (1982); M. Kohmoto, Annals of Physics **160**, 343 (1985).
- [5] F. D. M. Haldane, Phys. Rev. Lett. **61**, 2015 (1988).
- [6] I. Dzyaloshinsky, J. Phys. Chem. Solids **4**, 241 (1958); T. Moriya, Phys. Rev. **120**, 91 (1960).
- [7] H. Katsura, N. Nagaosa, and P. A. Lee, Phys. Rev. Lett. **104**, 066403 (2010).
- [8] R. Matsumoto and S. Murakami, Phys. Rev. Lett. **106**, 197202 (2011); Phys. Rev. B **84**, 184406 (2011).
- [9] L. Zhang, J. Ren, J. S. Wang, and B. Li, Phys. Rev. B **87**, 144101 (2013).
- [10] R. Shindou, R. Matsumoto, S. Murakami, and J. I. Ohe, Phys. Rev. B **87**, 174427 (2013).
- [11] R. Matsumoto, R. Shindou, and S. Murakami, Phys. Rev. B **89**, 054420 (2014).
- [12] A. Mook, J. Henk, and I. Mertig, Phys. Rev. B **90**, 024412 (2014); A. Mook, J. Henk, and I. Mertig, Phys. Rev. B **89**, 134409 (2014).
- [13] H. Lee, J. H. Han, and P. A. Lee, Phys. Rev. B. **91**, 125413 (2015).
- [14] S. A. Owerre, J. Phys.: Condens. Matter **28**, 386001 (2016).
- [15] S. A. Owerre, J. Appl. Phys. **120**, 043903 (2016).
- [16] M. Pereiro, D. Yudin, J. Chico, C. Etz, O. Eriksson, and A. Bergman, Nature Communications **5**, 4815 (2014).
- [17] A. A. Kovalev and V. Zyuzin, Phys. Rev. B **93**, 161106(R) (2016).
- [18] R. Chisnell, J. S. Helton, D. E. Freedman, D. K. Singh, R. I. Bewley, D. G. Nocera, and Y. S. Lee, Phys. Rev. Lett. **115**, 147201 (2015).
- [19] Max Hirschberger, Robin Chisnell, Young S. Lee, and N. P. Ong, Phys. Rev. Lett. **115**, 106603 (2015).
- [20] Y. Onose, T. Ideue, H. Katsura, Y. Shiomi, N. Nagaosa, Y. Tokura, Science **329**, 297 (2010).
- [21] T. Ideue, Y. Onose, H. Katsura, Y. Shiomi, S. Ishiwata, N. Nagaosa, and Y. Tokura, Phys. Rev. B. **85**, 134411 (2012).
- [22] D. Watanabe, K. Sugii, M. Shimozawa, Y. Suzuki, T. Yajima, H. Ishikawa, Z. Hiroi, T. Shibauchi, Y. Matsuda, M. Yamashita, Proc. Natl. Acad. Sci. USA **113**, 8653 (2016).
- [23] C. Balz, B. Lake, J. Reuther, H. Luetkens, R. Schönemann, Th. Herrmannsdörfer, Y. Singh, A. T. M. Nazmul Islam, E. M. Wheeler, J. A. Rodriguez-Rivera, T. Guidi, G. G. Simeoni, C. Baine, and H. Ryll, arXiv:1606.06463; Nature Physics (2016).
- [24] P. Mendels, A. Olariu, F. Bert, D. Bono, L. Limot, G. Collin, B. Ueland, P. Schiffer, R. J. Cava, N. Blanchard, F. Duc, and J. C. Trombe, J. Phys.: Condens. Matter **19**, 145224 (2007).
- [25] M. Yoshida, M. Takigawa, H. Yoshida, Y. Okamoto, and Z. Hiroi, Phys. Rev. Lett. **103**, 077207 (2009).
- [26] M. Yoshida, M. Takigawa, S. Kramer, S. Mukhopadhyay, M. Horvatic, C. Berthier, H. Yoshida, Y. Okamoto, Z. Hiroi, J. Phys. Soc. Jpn. **81**, 024703 (2012).
- [27] M. Elhajal, B. Canals, and C. Lacroix, Phys. Rev. B **66**, 014422 (2002).
- [28] K. Matan, D. Grohol, D. G. Nocera, T. Yildirim, A. B. Harris, S. H. Lee, S. E. Nagler, and Y. S. Lee, Phys. Rev. Lett. **96**, 247201 (2006).
- [29] O. Cépas, C. M. Fong, P. W. Leung, and C. Lhuillier Phys. Rev. B **78**, 140405(R) (2008).
- [30] A. Zorko, S. Nellutla, J. van Tol, L. C. Brunel, F. Bert, F. Duc, J.-C. Trombe, M. A. de Vries, A. Harrison, and P. Mendels, Phys. Rev. Lett. **101**, 026405 (2008).
- [31] H. Yoshida, Y. Michiue, E. Takayama-Muromachi, and M. Isobe, J. Mater. Chem. **22**, 18793 (2012).
- [32] A. Zorko, F. Bert, A. Ozarowski, J. van Tol, D. Boldrin, A. S. Wills, and P. Mendels, Phys. Rev. B **88**, 144419 (2013).
- [33] A. L. Chernyshev, Phys. Rev. B **92**, 094409 (2015).
- [34] T. Holstein and H. Primakoff, Phys. Rev. **58**, 1098 (1940).
- [35] S. A. Owerre, arXiv:1608.00545 (2016).

Field-Induced Magnon Hall Effect in Kagomé Antiferromagnet: Supplemental Material

S. A. Owerre

¹*Perimeter Institute for Theoretical Physics, 31 Caroline St. N., Waterloo, Ontario N2L 2Y5, Canada.*

²*African Institute for Mathematical Sciences, 6 Melrose Road, Muizenberg, Cape Town 7945, South Africa.*

At zero magnetic field, the transverse thermal Hall conductivity vanishes for fully antiferromagnetic quantum systems with Néel-like magnetic ordering. The presence of a nonzero magnetic field gives rise to a canted ordering with finite thermal Hall conductivity. We have analyzed a similar problem in the frustrated honeycomb lattice [1]. Here, we present the analysis for the Kagomé antiferromagnet. We consider the Hamiltonian

$$H = \sum_{i,j} J_{ij} \mathbf{S}_i \cdot \mathbf{S}_j + \sum_{\langle i,j \rangle} \mathbf{D}_{ij} \cdot \mathbf{S}_i \times \mathbf{S}_j - h \sum_i S_{iz}, \quad (11)$$

where $J_{ij} > 0$ are the isotropic antiferromagnetic couplings for nearest- (NN) and next-neighbours (NNN), \mathbf{D}_{ij} is the DMI between sites i and j , and h is the magnetic field in units of $g\mu_B$. At zero field, the $\mathbf{q} = 0$ ground state in which the spins are oriented 120° apart is stabilized by the next-nearest-neighbour exchange [2] or the symmetry breaking out-of-plane DMI, $\mathbf{D}_{ij} = (0, 0, \mp D_z)$ [3], where $-/+$ denotes the directions of the out-of-plane DMI in the up/down triangles as depicted in Fig. 8. The magnon excitations of this ordered state are known both experimentally and theoretically [4, 5]. It consists of one flat band (induced by the DMI) and two dispersive bands which are gapless at $\mathbf{K} = (\pm 2\pi/3, 0)$ point in the first Brillouin zone. As shown in the main text, such magnon excitations are trivial and do not yield any topological effect, hence thermal Hall conductivity vanishes for such systems.

For nonzero magnetic field, this system has not been studied at least in the topological context. In this case, the coplanar 120° Néel order is expected to cant in the direction of the field. To study the excitations of this system, we assume that the spins lie on the x - y Kagomé plane at zero field and perform a $2\pi/3$ rotation about the z -axis on sublattices B and C [2], followed by a rotation about the y -axis with the canting angle χ . The total rotation matrix is given by

$$\mathcal{R}_z(\theta_i) \cdot \mathcal{R}_y(\chi) = \begin{pmatrix} \cos \theta_i \cos \chi & -\sin \theta_i & \cos \theta_i \sin \chi \\ \sin \theta_i \cos \chi & \cos \theta_i & \sin \theta_i \sin \chi \\ -\sin \chi & 0 & \cos \chi \end{pmatrix}, \quad (12)$$

where θ_i labels the angles in each sublattice with $\theta_A = 0$ and $\theta_{B,C} = \pm 2\pi/3$, χ is the canting angle, and $\mathbf{D}_{ij} = (0, 0, -D_z)$ is the out-of-plane DMI. We perform the rotation

$$\mathbf{S}_i = \mathcal{R}_z(\theta_i) \cdot \mathcal{R}_y(\chi) \cdot \mathbf{S}'_i, \quad (13)$$

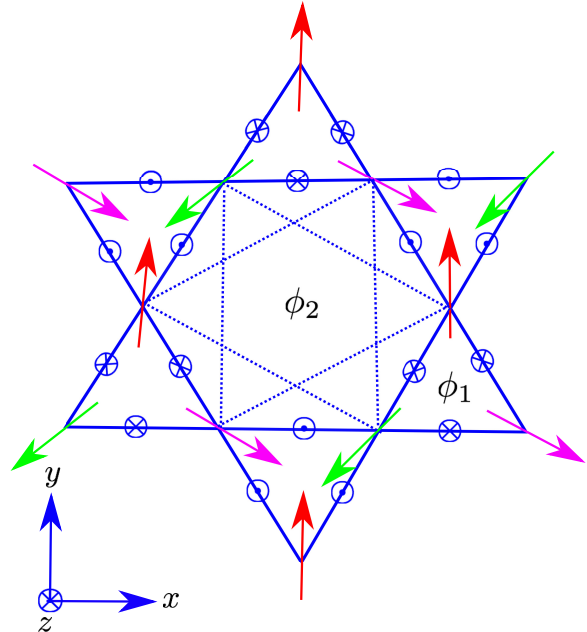


FIG. 8: Color online. The zero field coplanar 120° on the Kagomé lattice corresponding to the $\mathbf{q} = 0$ ground state of Kagomé antiferromagnet in the presence of an out-of-plane DMI. The dashed triangle connects the next-nearest-neighbours. At nonzero field each spin cant by an angle χ with respect to the field. The coloured arrows denote different sublattices and $\phi_{1,2}$ are the field-induced fictitious fluxes on the NN and NNN triangular plaquettes.

and drop the prime in the corresponding Hamiltonian to obtain

$$H_{J_1} = J_1 \sum_{\langle i,j \rangle} \left[\cos \theta_{ij} \mathbf{S}_i \cdot \mathbf{S}_j + \sin \theta_{ij} \cos \chi (\mathbf{S}_i \times \mathbf{S}_j)_z \right. \quad (14)$$

$$\left. + 2 \sin^2 \left(\frac{\theta_{ij}}{2} \right) [\sin^2 \chi S_{ix} S_{jx} + \cos^2 \chi S_{iz} S_{jz}] \right],$$

$$H_{J_2} = J_2 \sum_{\langle\langle i,j \rangle\rangle} \left[\cos \theta_{ij} \mathbf{S}_i \cdot \mathbf{S}_j + \sin \theta_{ij} \cos \chi (\mathbf{S}_i \times \mathbf{S}_j)_z \right. \quad (15)$$

$$\left. + 2 \sin^2 \left(\frac{\theta_{ij}}{2} \right) [\sin^2 \chi S_{ix} S_{jx} + \cos^2 \chi S_{iz} S_{jz}] \right],$$

$$H_{DMI} = D_z \sum_{\langle i,j \rangle} \left[\sin \theta_{ij} [\cos^2 \chi S_{ix} S_{jx} + S_{iy} S_{jy} + \sin^2 \chi S_{iz} S_{jz}] - \cos \theta_{ij} \cos \chi (\mathbf{S}_i \times \mathbf{S}_j)_z \right], \quad (16)$$

$$H_z = -h \cos \chi \sum_i S_{iz}. \quad (17)$$

The canting angle is determined from the classical energy

$$E_{cl}/S^2 = \sum_{i,j} \left[2J \sin^2 \left(\frac{\theta_{ij}}{2} \right) \cos^2 \chi + J \cos \theta_{ij} + D_z \sin^2 \chi \sin \theta_{ij} \right] - \frac{h}{S} \sum_i \cos \chi, \quad (18)$$

where $J = J_1 + J_2$. For the coplanar 120° Néel order, the classical energy is given by

$$E_{cl}/3NS^2 = 2J \left(-\frac{1}{2} + \frac{3}{2} \cos^2 \chi \right) - \sqrt{3} D_z \sin^2 \chi - \frac{h}{S} \cos \chi. \quad (19)$$

Minimizing this energy yields the canting angle $\cos \chi = h/h_s$, with $h_s = (6J + \sqrt{3}D_z)S$. At zero field, we recover the fact that the spins are on the Kagomé plane $\chi = \pi/2$.

The antiferromagnetic system differs from the ferromagnetic system [6–10] in two respects. Firstly, at zero field $\chi = \pi/2$ the coefficient of the chiral term $(\mathbf{S}_i \times \mathbf{S}_j)_z$ vanishes and the system is topologically trivial as mentioned above. As we shall show, a nonzero field induces nontrivial bands in the antiferromagnetic system. Secondly, the classical energy depends on the DMI as it contributes to the ground state ordering of the system. This is not the case in ferromagnets. We proceed as usual by introducing the Holstein-Primakoff spin bosonic operators $S_{ix} = \sqrt{S/2}(b_i^\dagger + b_i)$, $S_{iy} = i\sqrt{S/2}(b_i^\dagger - b_i)$ and $S_{iz} = S - b_i^\dagger b_i$, the magnon tight binding Hamiltonian is given by

$$H_2 = S \sum_{i,j} \left[-\Delta_{ij}^z (b_i^\dagger b_i + b_j^\dagger b_j) + \Delta_{ij} (e^{-i\phi_{ij}} b_i^\dagger b_j + h.c.) + \Delta'_{ij} (b_i^\dagger b_j^\dagger + h.c.) \right] + Sh_\chi \sum_i b_i^\dagger b_i, \quad (20)$$

where

$$\Delta_{ij}^z = (J_1 + J_2) (\cos \theta_{ij} + 2 \cos^2 \chi \sin^2(\theta_{ij}/2)) + D_z \sin^2 \chi \sin \theta_{ij} \quad (21)$$

$$\Delta_{1,ij} = \sqrt{(\Delta_{1,ij}^R)^2 + (\Delta_{1,ij}^M)^2}, \quad (22)$$

$$\Delta_{2,ij} = \sqrt{(\Delta_{2,ij}^R)^2 + (\Delta_{2,ij}^M)^2} \quad (23)$$

$$\Delta_{1,ij}^R = J_1 \left[\cos \theta_{ij} + \frac{2 \sin^2 \chi \sin^2(\theta_{ij}/2)}{2} \right] + D_z \sin \theta_{ij} \left(1 - \frac{\sin^2 \chi}{2} \right), \quad (24)$$

$$\Delta_{1,ij}^M = \cos \chi (J_1 \sin \theta_{ij} - D_z \cos \theta_{ij}), \quad (25)$$

$$\Delta_{2,ij}^R = J_2 \left[\cos \theta_{ij} + \frac{2 \sin^2 \chi \sin^2(\theta_{ij}/2)}{2} \right], \quad (26)$$

$$\Delta_{2,ij}^M = J_2 \cos \chi \sin \theta_{ij}, \quad (27)$$

$$\Delta'_{1,ij} = \frac{\sin^2 \chi}{2} (2J_1 \sin^2(\theta_{ij}/2) - D_z \sin \theta_{ij}) \quad (28)$$

$$\Delta'_{2,ij} = J_2 \sin^2 \chi \frac{2 \sin^2(\theta_{ij}/2)}{2}, \quad (29)$$

and $h_\chi = h \cos \chi$, $\tan \phi_{1,ij} = \Delta_{1,ij}^M / \Delta_{1,ij}^R$, $\tan \phi_{2,ij} = \Delta_{2,ij}^M / \Delta_{2,ij}^R$. The NNN fictitious flux ϕ_2 does not depend on the DMI and originates from the chiral term in the J_2 coupling. Notice that both fluxes do not vanish at zero DMI unlike in ferromagnets. In momentum space we obtain

$$H_2 = S \sum_{\mathbf{k}, \alpha, \beta; 1,2} (C_{\alpha\beta}^0 \delta_{\alpha\beta} + 2C_{\alpha\beta;1,2}) b_{\mathbf{k}\alpha}^\dagger b_{\mathbf{k}\beta} + C'_{\alpha\beta;1,2} (b_{\mathbf{k}\alpha}^\dagger b_{-\mathbf{k}\beta}^\dagger + b_{\mathbf{k}\alpha} b_{-\mathbf{k}\beta}), \quad (30)$$

where $\alpha, \beta = A, B, C$ and the coefficients are given by

$$\mathbf{C}_0 = \text{diag}(\zeta_{AA}, \zeta_{BB}, \zeta_{CC}), \quad (31)$$

with $\zeta_{\alpha\alpha} = h_\chi - \sum_{\alpha\beta} z_{\alpha\beta} \Delta_{\alpha\beta}^z$ and $z_{\alpha\beta}$ is the number of β sublattice nearest (next-nearest) to α sublattice.

$$\mathbf{C}_{1,2} = \Delta_{1,2;\alpha\beta} \begin{pmatrix} 0 & \gamma_{AB}^{1,2} e^{-i\phi_{1,2}} & \gamma_{CA}^{1,2} e^{i\phi_{1,2}} \\ \gamma_{AB}^{*1,2} e^{i\phi_{1,2}} & 0 & \gamma_{BC}^{1,2} e^{-i\phi_{1,2}} \\ \gamma_{CA}^{*1,2} e^{-i\phi_{1,2}} & \gamma_{BC}^{*1,2} e^{i\phi_{1,2}} & 0 \end{pmatrix}; \quad (32)$$

$$\mathbf{C}'_{1,2} = \Delta'_{1,2;\alpha\beta} \begin{pmatrix} 0 & \gamma_{AB}^{1,2;\alpha\beta} & \gamma_{CA}^{1,2} \\ \gamma_{AB}^{*1,2} & 0 & \gamma_{BC}^{1,2} \\ \gamma_{CA}^{*1,2} & \gamma_{BC}^{*1,2} & 0 \end{pmatrix}; \quad (33)$$

where $\gamma_{AB}^1 = \cos k_1$, $\gamma_{BC}^1 = \cos k_2$, $\gamma_{CA}^1 = \cos k_3$; $\gamma_{AB}^2 = \cos p_1$, $\gamma_{BC}^2 = \cos p_2$, $\gamma_{CA}^2 = \cos p_3$ and $k_i = \mathbf{k}_i \cdot \mathbf{a}_i$, $p_i = \mathbf{k}_i \cdot \mathbf{b}_i$, $\mathbf{a}_1 = (1, 0)$, $\mathbf{a}_2 = (-1/2, \sqrt{3}/2)$, $\mathbf{a}_3 = (-1/2, -\sqrt{3}/2)$, $\mathbf{b}_1 = \mathbf{a}_3 - \mathbf{a}_2$, $\mathbf{b}_2 = \mathbf{a}_1 - \mathbf{a}_3$, $\mathbf{b}_3 = \mathbf{a}_2 - \mathbf{a}_1$. Here, $\zeta_{\alpha\alpha}$, $\Delta_{1,2;\alpha\beta}$ and $\Delta'_{1,2;\alpha\beta}$ are all the same for the coplanar 120° Néel order with $\theta_A = 0$ and $\theta_{B,C} = \pm 2\pi/3$.

The Hamiltonian can be written in terms of the Nambu operators

$$H_2 = \mathcal{E}_0 + S \sum_{\mathbf{k}} \Psi_{\mathbf{k}}^\dagger \mathcal{H}(\mathbf{k}) \Psi_{\mathbf{k}}, \quad (34)$$

where $\Psi_{\mathbf{k}}^\dagger = (b_{\mathbf{k}A}^\dagger, b_{\mathbf{k}B}^\dagger, b_{\mathbf{k}C}^\dagger, b_{-\mathbf{k}A}, b_{-\mathbf{k}B}, b_{-\mathbf{k}C})$. The Hamiltonian to be diagonalized is given by

$$\mathcal{H}(\mathbf{k}) = \begin{pmatrix} \mathbf{c}_0/2 + \mathbf{c}_1 + \mathbf{c}_2 & \mathbf{c}'_1 + \mathbf{c}'_2 \\ \mathbf{c}'_1 + \mathbf{c}'_2 & \mathbf{c}_0/2 + \mathbf{c}_1 + \mathbf{c}_2 \end{pmatrix}. \quad (35)$$

[1] S. A. Owerre, arXiv:1608.00545 (2016).

[2] A. B. Harris, C. Kallin, and A. J. Berlinsky, Phys. Rev. B **45**, 2899 (1992).

[3] M. Elhajal, B. Canals, and C. Lacroix, Phys. Rev. B **66**, 014422 (2002).

[4] K. Matan, D. Grohol, D. G. Nocera, T. Yildirim, A. B. Harris, S. H. Lee, S. E. Nagler, and Y. S. Lee, Phys. Rev. Lett. **96**, 247201 (2006).

[5] A. L. Chernyshev, Phys. Rev. B **92**, 094409 (2015).

[6] H. Katsura, N. Nagaosa, and P. A. Lee, Phys. Rev. Lett. **104**, 066403 (2010).

[7] R. Matsumoto and S. Murakami, Phys. Rev. Lett. **106**, 197202 (2011); Phys. Rev. B **84**, 184406 (2011).

[8] L. Zhang, J. Ren, J. S. Wang, and B. Li, Phys. Rev. B **87**, 144101 (2013).

[9] A. Mook, J. Henk, and I. Mertig, Phys. Rev. B **90**, 024412 (2014); A. Mook, J. Henk, and I. Mertig, Phys. Rev. B **89**, 134409 (2014).

[10] H. Lee, J. H. Han, and P. A. Lee, Phys. Rev. B. **91**, 125413 (2015).